Chemical Physics 534 (2020) 110753

Contents lists available at ScienceDirect

Chemical Physics

journal homepage: www.elsevier.com/locate/chemphys

Ethanol electrooxidation on highly active palladium/graphene oxide aerogel catalysts

Jing Zhang[a], Zhiliang Zhao[a], Yongzhao Wang[b], Juan Wang[a,*], Dengchao Peng[a], Baiyu Li[c], Tingting Bo[a], Kang Zheng[a], Zhiyuan Zhou[a], Lin Lv[a], Zhiling Xin[a,*], Bingsen Zhang[b,*], Lidong Shao[a,*]

[a] Shanghai Key Laboratory of Materials Protection and Advanced Materials in Electric Power, Shanghai University of Electric Power, 2103 Pingliang Road, Shanghai 200090, China
[b] Shenyang National Laboratory for Materials Science Institute of Metal Research, Chinese Academy of Sciences, 72 Wenhua Road, Shenyang 110016, China
[c] Nantong Vocational University, 89 Qingnian Road, Nantong 226006, China

ARTICLE INFO

Keywords:
Pd nanoparticles
Ethanol oxidation reaction
Graphene oxide
Aerogels
Functional groups

ABSTRACT

In this work, the low-loading (3 wt%) palladium/graphene oxide (Pd/GO) aerogels are facilely prepared via the lyophilisation, vacuum and reduction treatments. The Pd/GO aerogels display enhanced activity and stability in comparison to the commercial Pd/C. The enhancement of electrocatalytic performance can be attributed to the functional groups on the surfaces of the GO support, such as carbonyl and carboxyl groups, which can be tuned to interact with palladium to form active phases for the reaction. In addition, Pd nanoparticles (NPs) remain dispersed in nanoscale on the reacted catalyst.

1. Introduction

Fuel cells are widely studied for environmentally friendly power generation because they are capable of directly and conveniently converting chemical energy into electrical energy. Direct ethanol fuel cells (DEFCs) are remarkable due to their high current density and the fact that ethanol is an abundant and low-cost liquid fuel [1]. Thus, the design and preparation of a superior electrocatalyst has become vital for producing DEFCs [2]. In the current DEFCs, the anode catalysts are generally based on either Pd or Pt. The Pd-based electrocatalysts are not only low-cost, but also display higher ethanol oxidation reaction (EOR) activity [3–9] and superior anti-CO poisoning characteristics [10–11] than the Pt-based catalysts in an alkaline medium.

The support materials play a key role in the design of the catalysts for the EOR. Carbon materials with excellent physicochemical properties and unique structures are very attractive as supports for DEFCs palladium-containing electrocatalysts [12–17]. Among the numerous carbon materials, graphene with the atomic layer of sp^2 C-bonded two-dimensional (2D) nanosheets is universally considered to be a prospective catalyst supporting material due to its high conductivity [18–19]. This not only helps to maximise the electron transfer rate on the surface of the nanoelectrocatalyst, but also provides better mass transfer of reactants to the electrocatalyst. Furthermore, the surface chemistry of carbon is also a significant aspect to consider when designing highly active catalysts [20–22]. The functional groups on the support materials can promote the catalytic reaction by affecting the electronic structure of the loaded metal particles. The outer surface of graphene can be chemically modified by introducing oxygen-containing functional groups such as carboxyl, carbonyl, and hydroxyl by an oxidation treatment. Based on interaction between the metal and support [23–24], Pd nanostructures can be anchored on the oxygen-containing functional groups by effectively forming a stable metal bond through electrostatic interaction.

In this work, the low-loading (3 wt%) Pd/GO aerogels, with large surface areas and enrich functionalities, are prepared by the lyophilisation, vacuum and reduction treatments. Functional groups on the GO surface can help anchor Pd nanoparticles (NPs) and inhibit particle aggregation, thereby achieving nanoscale uniform dispersion of Pd NPs. The Pd/GO aerogels displayed higher activity and stability than the commercial Pd/C in EOR. The fresh and reacted catalysts were analyzed to study the correlation between structure and performance.

2. Experimental

The graphene oxide (GO) is from Tanyuan Co. Ltd (Shanghai). The $Pd(NO_3)_2$ (10 wt% in 10 wt% HNO_3), Pd/C (3 wt%) and Nafion (5 wt%)

* Corresponding authors.
E-mail addresses: wangjuan@shiep.edu.cn (J. Wang), xinzhiling@126.com (Z. Xin), bszhang@imr.ac.cn (B. Zhang), lidong.shao@shiep.edu.cn (L. Shao).

https://doi.org/10.1016/j.chemphys.2020.110753
Received 27 January 2020; Received in revised form 10 March 2020; Accepted 11 March 2020
Available online 12 March 2020
0301-0104/

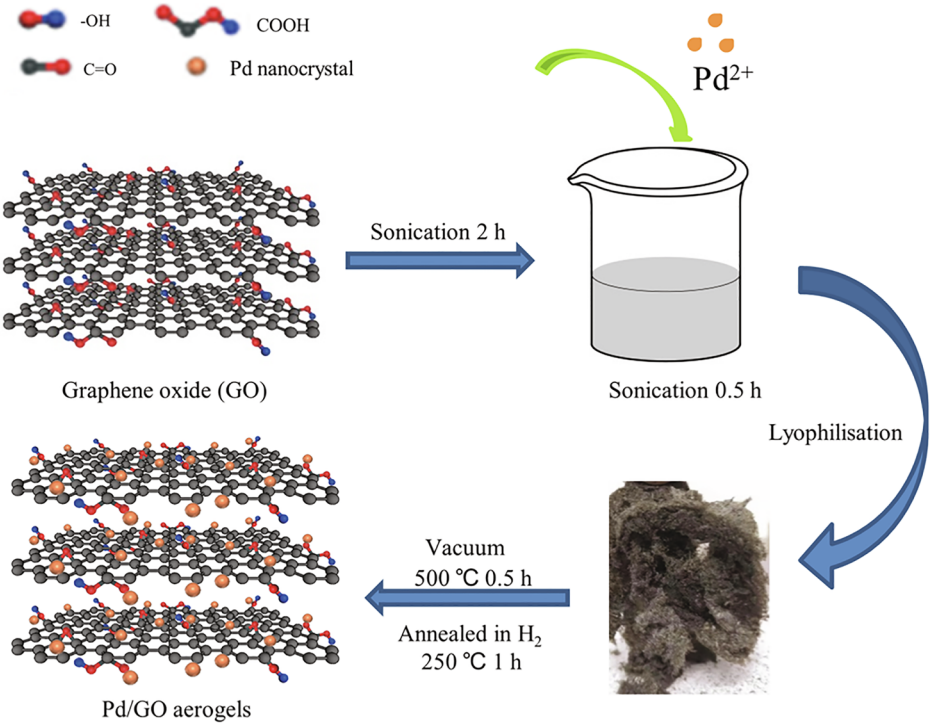

Fig. 1. Schematic diagram of the preparation of the Pd/GO aerogels.

are purchased from Sigma Aldrich. The ethanol (> 99.7%) and KOH are supplied by Sinopharm Co. Ltd (China). The hydrogen (H_2, 99.99%), helium (He, 99.99%) and nitrogen (N_2, 99.99%) are purchased from Weichuang Co. Ltd (Shanghai). The experimental water is Millipore ultrapure water.

Fig. 1 is a schematic diagram of the preparation of the Pd/GO aerogels. Firstly, the raw GO solution was stirred for 2 h while undergoing sonication, $PdNO_3$ solution was then added whilst undergoing sonication for 0.5 h. After 2.5 h of sonication, the cations were deposited on the surface of the support meanwhile the interlayer spacing of the raw GO increased. Subsequently, the mixed solution was dried by lyophilisation (freeze drying) to maintain the integrity of the morphology. The interlayer spacing was further expanded after vacuum treatment at 500 °C at a heating rate of 10 °C/min for 0.5 h. Finally, the cations were reduced by H_2 through an annealing treatment at 250 °C at a heating rate of 3 °C/min for 1 h to form Pd nanocrystals. Notably, as shown in Fig. 2, the Pd/GO aerogels obtained after the vacuum and hydrogen reduction treatment still maintained a good two-dimensional morphology. Supporting Information provides experimental details information for sample preparation and electrochemical measurements.

Field emission transmission electron microscopy (TEM, FEI Tecnai G2 F20) images were employed in scanning TEM (STEM) mode to characterise the morphologies and microstructures of the catalysts. The morphology of the catalysts was characterised using scanning electron microscopy (SEM, JSM 6701F). X-ray photoelectron spectroscopy (XPS) was carried out by a Thermo ESCALAB 250 instrument using an Al Kα radiation source. X-ray diffraction (XRD) analyses were performed on a Bruker D8 Advance instrument employing Cu Ka radiation. Raman spectra were performed on a HORIBA LabRAM HR Evolution Raman spectrometer at an excitation wavelength of 633 nm with an Ar-ion laser.

3. Results and discussion

Fig. 2a shows the typical STEM images of Pd/GO aerogels, the Pd NPs are uniformly and well dispersed on the support, indicating the anchoring effect from the graphene oxide. The inset of Fig. 2a shows the particle size distribution of the Pd NPs. From statistical analysis, the average diameter of Pd NPs is ca. 2.95 nm. However, in the case of the Pd/C (shown in Fig. S1), the mean size of metal particles is ca. 3.53 nm. The TEM image of the well-dispersed Pd/GO aerogels is shown in Fig. 2b. From the energy-dispersive X-ray spectroscopy (EDX) elemental mapping images (Fig. 2e-g), it can be seen that there is a homogeneous distribution of Pd and O over the surfaces of the Pd/GO aerogel catalysts. In order to demonstrate the fine structure of the samples, high-resolution transmission electron microscopy (HRTEM) was performed with corresponding local Fast Fourier Transformation (FFT). As shown in Fig. 2h, the lattice fringes Pd (1 1 1) and Pd (2 0 0) with d-spacing of 2.24 and 1.94 Å can be identified in the Pd/GO aerogel samples referring to JCPDS NO. 65–6174. Fig. 2i shows the SEM image of the Pd/GO aerogels, which evidences the two-dimensional sheet morphology of the Pd/GO aerogels.

Fig. 3A shows the XRD of the (a) Pd/C and (b) Pd/GO aerogels and provides information on the crystallographic structures. The broad diffraction peak at 24.46° is consistent with the (0 0 2) plane of a carbonaceous structure. Meanwhile, the characteristic diffraction peaks located at 40.00°, 46.53°, 67.92°, and 81.85° correspond, respectively, to the (1 1 1), (2 0 0), (2 2 0), and (3 1 1) crystalline planes of the metallic Pd (JCPDS No. 88–2235). For the Pd/GO aerogels, the strength of the Pd peaks is not obvious due to the NPs size of the metal was too tiny [25], which is consistent with the TEM results.

Raman spectroscopy was used to rapidly detect the structural features of the carbonaceous catalysts and qualitatively characterise them. Fig. 3B shows the Raman spectra of (a) Pd/GO aerogels and (b) Pd/C, which demonstrates the disorder and defects of the carbon structure. Both catalysts have two evident bands, namely the G and the D band at 1598 and 1325 cm^{-1}. The D-band originates from defects in the graphite plane [26], and the G-band corresponds to the vibration of the sp^2-bonded carbon domains [27]. The intense G band in the Pd/GO aerogels indicates that the catalyst remains in the graphite structure after vacuum annealing at 500 °C. The value of I_D/I_G is generally used to reveal the amount of in-plane and edge flaws of the catalysts [28]. The I_D/I_G value (1.28) for Pd/GO aerogels is slightly higher than the value for Pd/C (1.13), suggesting that there are planar lattice defects in

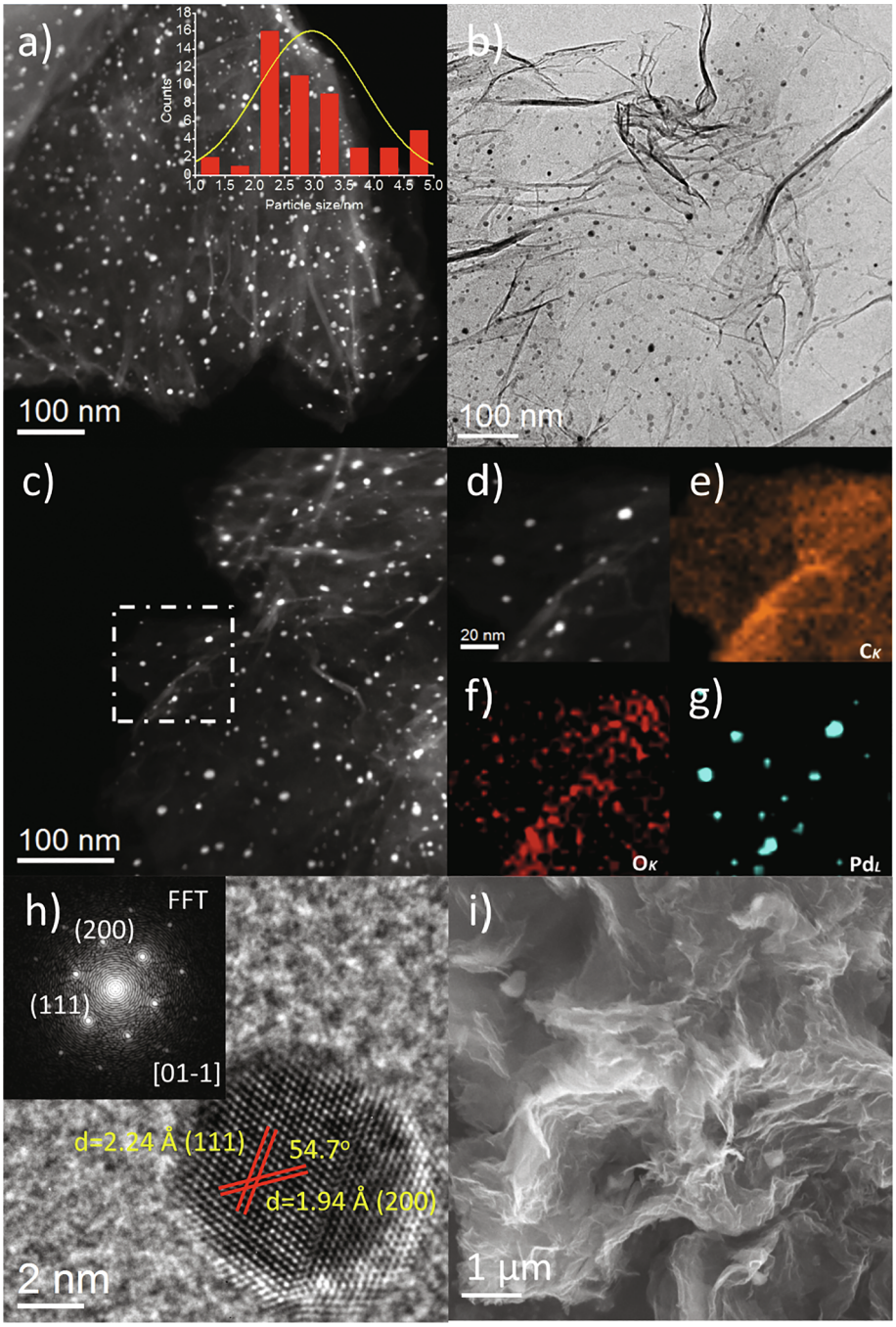

Fig. 2. (a) Typical STEM image of the Pd/GO aerogels with the inset shows the Pd particle size distribution. (b) TEM image of the Pd/GO aerogels. (c)-(g) EDX elemental maps of (e) C, (f) O and (g) Pd in the Pd/GO aerogels. (h) HRTEM image of the Pd/GO aerogels with FFT. (i) SEM image of the Pd/GO aerogels.

the Pd/GO aerogels.

XPS was utilised to inspect the valence of the elements and the properties of the Pd/GO aerogels at the surface and subsurface regions. In the fitted Pd 3d spectrum of the Pd/GO aerogels (Fig. 4a), the Pd $3d_{5/2}$ (335.68 eV) and Pd $3d_{3/2}$ (340.86 eV) peaks are assigned to Pd^0, while the Pd $3d_{5/2}$ (337.16 eV) and Pd $3d_{3/2}$ (342.36 eV) peaks are both ascribed to Pd^{2+} [29–30]. The remaining two peaks at 338.13 and 343.35 eV are ascribed to the bivalent polynuclear Pd-hydroxo complexes due to the imcomplete reduction of the palladium salt [31]. As illustrated in Fig. 4b, the C 1 s spectrum of the Pd/GO aerogels is fitted to four independent peaks that represent different functional groups. The intense peak of 284.78 eV is attributed to the sp^3 hybrid C—C. The binding energy peak located at 285.69 eV corresponds to hydroxyl (C-OH), 287.12 eV corresponds to carbonyl (C═O), and 290.12 eV corresponds to carboxyl (COOH) [32–34]. Based on the deconvolution of the C 1 s peak, the percentage of total oxygen-containing groups of the Pd/GO aerogels is estimated to exceed 37%, which is higher than 19% of the Pd/C (as shown in Fig. S2).

Fig. 5A illustrates the cyclic voltammograms (CVs) of the Pd/GO aerogels and Pd/C conducted between −0.8 V and 0.6 V at 50 mV s^{-1} in 1 M KOH + 1 M ethanol solution while purging with nitrogen. Both catalysts show forward and backward peaks and the lower onset potential of the Pd/GO aerogels indicates that it is easier to achieve an EOR. As the CVs show, the EOR performance of the Pd/GO aerogels features a forward peak current density (I_f) around −0.2 V to ethanol oxidation, and the backward current density (I_b) around −0.5 V to

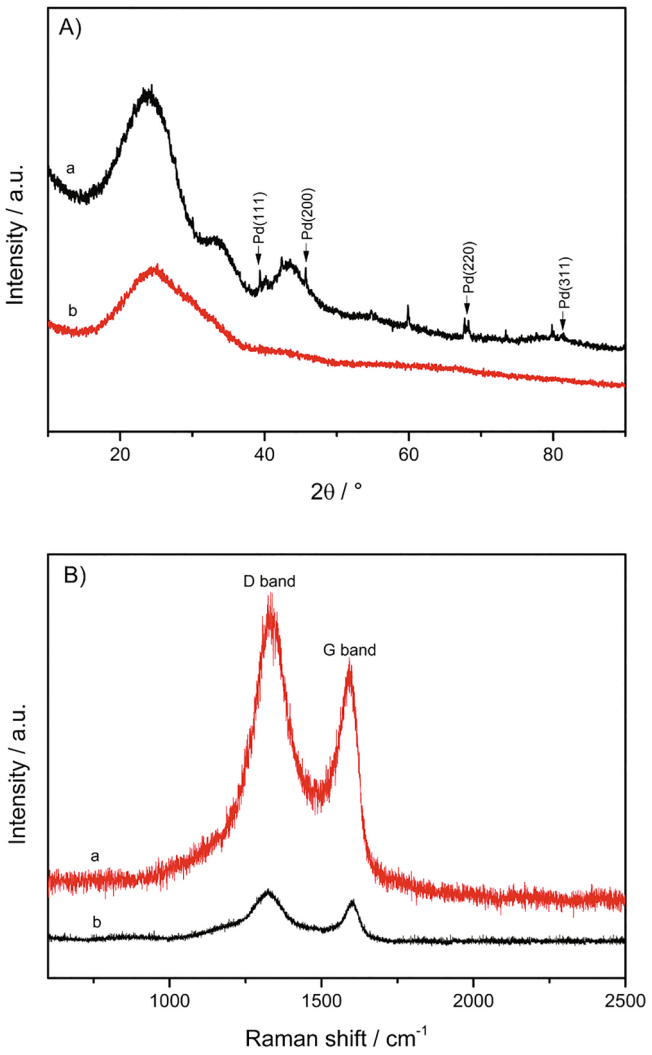

Fig. 3. (A) XRD patterns of (a) Pd/C and (b) Pd/GO aerogels. (B) Raman spectra of (a) Pd/GO aerogels and (b) Pd/C.

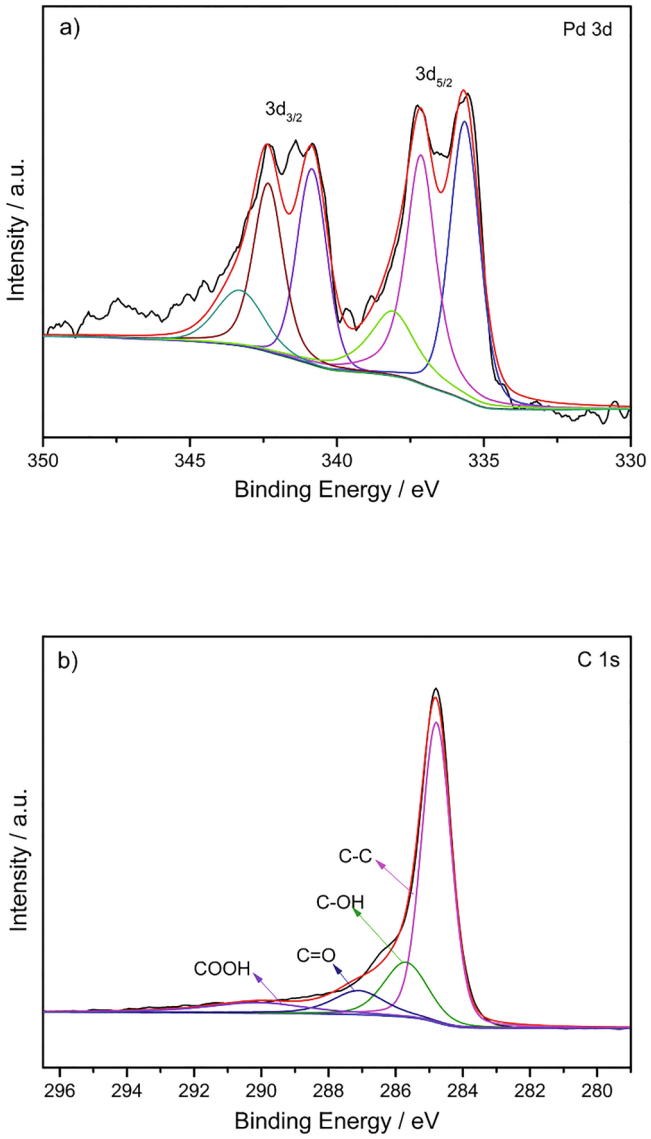

Fig. 4. (a) XPS spectrum of the Pd/GO aerogels in Pd 3d region. (b) XPS spectrum of the Pd/GO aerogels in C 1s region.

remove residual carbonaceous materials that were not totally oxidised. Understanding the mechanism of electroxidation of ethanol in detail is essential for the anode design of Pd-based DEFCs. Zhao et al. [35] has explored the mechanism of electroxidation of ethanol on palladium electrodes. It was found that the dissociative adsorption of ethanol proceeded quite quickly, and the rate-determining step was to remove the adsorbed ethoxy groups through the hydroxyl groups adsorbed on the surface of the Pd electrode (Eqs. (1)–(3)).

$$Pd + OH^- \rightarrow Pd\text{-}OH_{ads} + e^- \quad (1)$$

$$Pd\text{-}(CH_3CH_2OH)_{ads} + 3OH^- \rightarrow Pd\text{-}(COCH_3)_{ads} + 3H_2O + 3e^- \quad (2)$$

$$Pd\text{-}(COCH_3)_{ads} + Pd\text{-}OH_{ads} \rightarrow Pd\text{-}CH_3COOH + Pd \quad (3)$$

As demonstrated in Fig. 5A, the Pd/GO aerogels have a visible mass activity of 1300 A g^{-1}, which is 2.7 times higher than the 480 A g^{-1} for commercial Pd/C. The electrochemical active surface area (ECSA) was generally used to investigate the electrochemical active sites. The ECSAs of the Pd-based electrocatalysts are calculated as follows: ECSA = Q/(0.405 × m), where Q (mC) is the Coulomb charge defined by integrating the PdO reduction peak area, 0.405 (mC cm^{-1}) represents the charge required to reduce a PdO monolayer, and m (g) is the Pd loading on the glassy carbon electrode [36]. Fig. S3 shows the CV measurements in 1 M KOH, the calculated ECSAs for the Pd/GO aerogels and Pd/C equal 97.43 and 38.41 m^2 g^{-1}, respectively. Clearly, the Pd/GO aerogels have an ESCA that is 2.5 times larger than that for commercial Pd/C, thus increasing the electrochemical activity of the electrocatalyst. Furthermore, the peak current ratio of the forward scan (I_f) to backward scan (I_b), I_f/I_b, is usually used to investigate the ability of catalysts to withstand the poisoning of carbonaceous materials [37]. The I_f/I_b ratios of Pd/GO aerogels and Pd/C equal 1.96 and 0.58, respectively, which demonstrates that the Pd/GO aerogels have a stronger anti-poisoning ability.

In order to assess the stability of the Pd/GO aerogels, 3600 s chronoamperometric curves were acquired in 1 M KOH + 1 M ethanol at a potential of −0.2 V. As shown in Fig. 5B, the Pd/GO aerogel catalysts exhibit higher current densities both in the initial and final measurements, indicating that the performance of the Pd/GO aerogels in the EOR is superior to Pd/C. At first, the current density of the EOR on both catalysts decrease sharply, possibly owing to the accumulation of toxic intermediates and adsorption on the catalyst surface, which tends to stabilise after a certain period of time. In terms of the Pd/GO aerogels, in the first 1000 s, the mass activity is 132.1 A g^{-1}, and in the following 1000 s, the mass activity is 95.2 A g^{-1}. After 3600 s of the stability test, the mass activity of the Pd/GO aerogels is 71.6 A g^{-1}, which is higher than the Pd/C (17.4 A g^{-1}). These observations

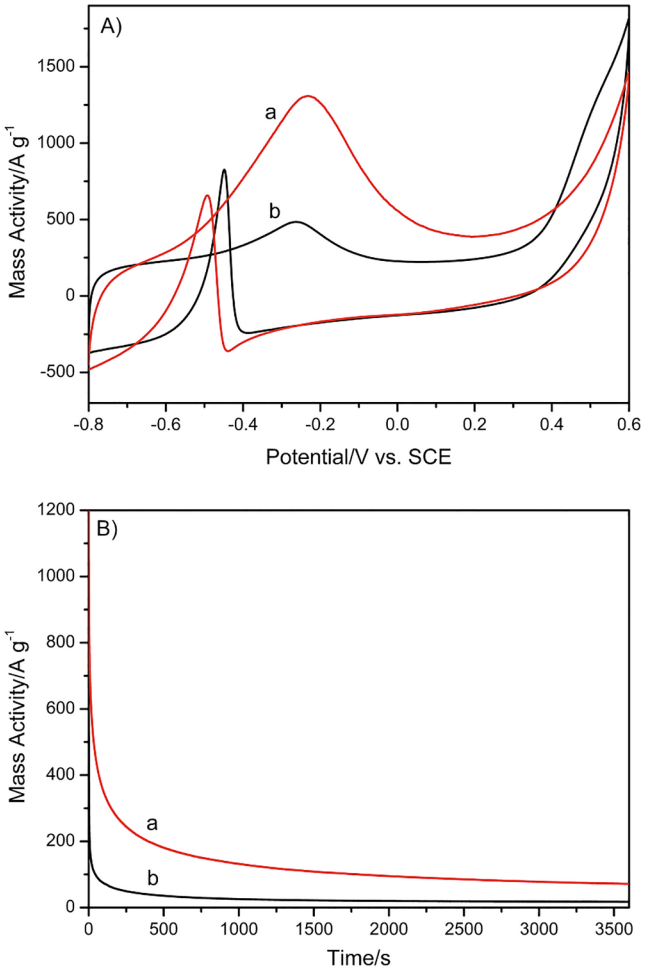

Fig. 5. (A) CV curves in 1 M KOH + 1 M ethanol at a scan rate of 50 mV s^{-1}. (B) chronoamperometric curves in 1 M KOH + 1 M Ethanol at a potential of −0.2 V vs. SCE, (a for Pd/GO aerogels and b for Pd/C).

indicate that Pd/GO aerogels have a relatively good stability towards EOR.

Fig. 6a and 6b show the representative TEM images of used Pd/GO aerogels, at different measurement scales. After 3600 s of the stability reaction, no significant morphological differences were observed. The Pd/GO aerogels still maintained a good two-dimensional morphology, meanwhile there was no obvious growth in the dimension of the Pd NPs after the reaction and a favourable distribution of particles was preserved. The inset of Fig. 6b shows the particle size distribution of the Pd NPs. The average dimension of the Pd NPs on the used catalysts increased slightly to ca. 3.79 nm, indicating that the Pd/GO aerogels had no significant particle agglomeration and metal leaching during the reaction.

Generally, graphene aerogels (GAs) can be prepared either by the polymerisation of an organogel or by assembling primary carbon nanomaterials [38]. Due to their excellent chemical durability and particular architecture, graphene aerogels have many extraordinary characteristics. GAs usually have an ultra-low density, their adjustable pore structures ensure a large internal surface area and low mass transfer resistance, and their carbon-based supports are an excellent way of transferring electrons. GAs also exhibit surprising catalytic activity [39]. In our work, the lyophilisation connected with the vacuum annealing ensures the integrity of the Pd/GO aerogels morphology and the uniform distribution of Pd NPs on the surface, the catalyst is free of surfactant formation process.

The elemental components of the Pd/GO aerogels and Pd/C determined using XPS are illustrated in Table S1. As can be seen from Table S1, the C 1s/O 1s ratio of the Pd/GO aerogels and Pd/C are 8.00 and 12.86, and the Pd^0/Pd^{2+} ratios are 1.04 and 3.64, respectively. Further calculations (Table S2) show that the oxygen-containing functional groups hydroxyl (C-OH), carbonyl (C═O), and carboxyl (COOH) groups of the Pd/GO aerogels account for 17.78%, 10.16%, and 9.08%, respectively, which are higher than 7.86%, 4.59% and 6.55% of the Pd/C. The percentage of total oxygen-containing groups of the Pd/GO aerogels is 37.13%, which is nearly double the Pd/C (19.00%). It is well known that functional groups can affect interactions with supported metal nanoparticles [40]. Here, we concluded that the O-containing functional groups, such as carbonyl and carboxyl, on the surface of GO are vital for the interaction of Pd with the support. It was reported that the lone pair of electrons around the C═O bond in the anhydride or carboxylic acid can be shared with the 4d orbital of Pd [41], which may result in an intense interaction between the Pd and GO. This possibly facilitates the anchoring of the Pd NPs, while also limiting the growth of the Pd NPs. Meanwhile, the particle size effects in Pd catalysis are closely related to the electrocatalytic performance [29,42]. The smaller particle size may contribute to relatively higher specific surface area and high exposed surface atoms density of Pd [43,44], which is of great significance for low-loading Pd-catalyzed ethanol oxidation. Moreover, the TEM images after the stability reaction further demonstrated the stability of the Pd/GO aerogels that we prepared. The Pd/GO aerogels still maintained the original morphology, while the size of Pd NPs did not increase significantly after the reaction, and still showed improved stability and dispersity, further confirming the intense interaction

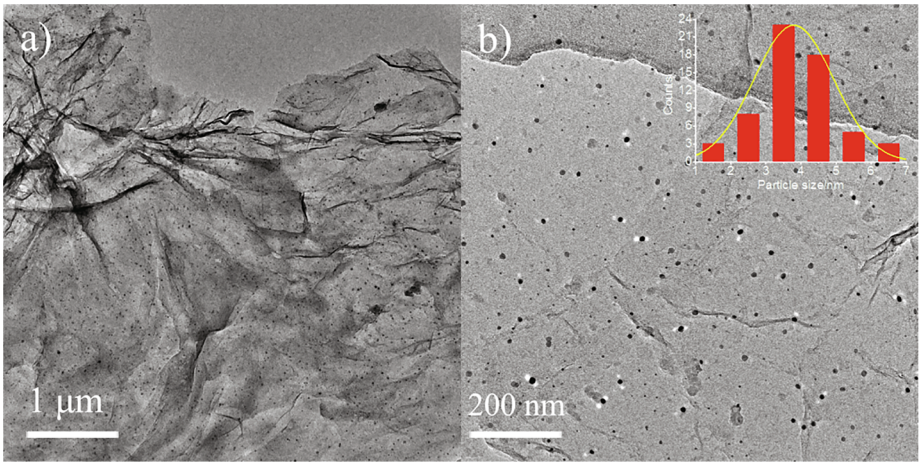

Fig. 6. (a), (b) TEM images of used Pd/GO aerogels with the inset of (b) shows the Pd particle size distribution.

between the Pd NPs and GO.

4. Conclusion

In summary, the low-loading (3 wt%) Pd/GO aerogels, with large surface areas and enrich functionalities, have been obtained aided by a relatively facile way combining the lyophilisation, vacuum, and reduction processing. The Pd/GO aerogels exhibit enhanced activity and stability compared with the commercial Pd/C. The GO with large surface provided a platform for immobilizing Pd NPs, on which the surface carbonyl and carboxyl groups promote the formation of active sites by forming the interaction between palladium and support. Due to the metal-support interaction, nanoscale Pd NPs on GO showed improved stability and dispersity after 3600 s reaction. Such a facile synthesis method can be used for a general catalyst development which exploits the role of enriched surface chemistry of aerogels in influencing catalysis.

CRediT authorship contribution statement

Jing Zhang: Writing - review & editing, Formal analysis, Investigation. **Zhiliang Zhao:** Data curation. **Yongzhao Wang:** Data curation, Software. **Juan Wang:** Writing - review & editing. **Dengchao Peng:** Visualization. **Baiyu Li:** Supervision. **Tingting Bo:** Data curation. **Kang Zheng:** Validation. **Zhiyuan Zhou:** Software. **Lin Lv:** Validation. **Zhiling Xin:** Supervision. **:** . **Bingsen Zhang:** Supervision, Funding acquisition. **Lidong Shao:** Conceptualization, Resources, Funding acquisition.

Declaration of Competing Interest

The authors declare that they have no known competing financial interests or personal relationships that could have appeared to influence the work reported in this paper.

Acknowledgements

This work was supported by the Science and Technology Commission of Shanghai Municipality (No. 14DZ2261000) and National Natural Science Foundation of China (No. 51802190).

Dr. Bingsen Zhang acknowledges the financial support provided by the National Natural Science Foundation of China (No. 51932005) and Liao Ning Revitalization.

Appendix A. Supplementary data

Supplementary data to this article can be found online at https://doi.org/10.1016/j.chemphys.2020.110753.

References

[1] L. An, T.S. Zhao, Transport phenomena in alkaline direct ethanol fuel cells for sustainable energy production, J. Power Sources 341 (2017) 199–211, https://doi.org/10.1016/j.jpowsour.2016.11.117.

[2] E. Antolini, Pt-Ni and Pt-M-Ni (M = Ru, Sn) anode catalysts for low-temperature acidic direct Alcohol Fuel Cells: A Review, Energies 10 (1) (2017) 1–20, https://doi.org/10.3390/en10010042.

[3] K. Jiang, P. Wang, S. Guo, X. Zhang, X. Shen, G. Lu, D. Su, X. Huang, Ordered PdCu-based nanoparticles as bifunctional oxygen-reduction and ethanol-oxidation electrocatalysts, Angew. Chem. Int. Ed. 55 (2016) 1–7, https://doi.org/10.1002/anie.201603022.

[4] C. Xu, Y. Liu, D. Yuan, Pt and Pd supported on carbon microspheres for alcohol electrooxidation in alkaline media, Int. J. Electrochem. Sci. 2 (2007) 647–680 http://citeseerx.ist.psu.edu/viewdoc/download?doi=10.1.1.653.6378&rep=rep1&type=pdf.

[5] W. Wang, W. Jing, L. Sheng, D. Chai, Y. Kang, Z. Lei, Pd_3Cu coupling with nitrogen-doped mesoporous carbon to boost performance in glycerol oxidation, Appl. Catal. A 538 (2017) 123–130, https://doi.org/10.1016/j.apcata.2017.03.027.

[6] W. Wang, Y. Dong, L. Xu, W. Dong, X. Niu, Z. Lei, Combining bimetallic-alloy with selenium functionalized carbon to enhance electrocatalytic activity towards glucose oxidation, Electrochim. Acta 244 (2017) 16–25, https://doi.org/10.1016/j.electacta.2017.05.078.

[7] H. Yang, S. Li, S. Shen, Z. Jin, J. Jin, J. Ma, Unraveling the cooperative synergy of palladium/tin oxide/aniline-functionalized carbon nanotubes enabled by layer-by-layer synthetic strategy for ethanol electrooxidation, ACS Sustainable Chem. Eng. 7 (2019) 10008–10015, https://doi.org/10.1021/acssuschemeng.9b01197.

[8] S. Li, H. Yang, H. Zou, M. Yang, X. Liu, J. Jin, J. Ma, Palladium nanoparticles anchored on the NCNTs@NGS with a three-dimensional sandwich-stacked framework as an advanced electrocatalyst for ethanol oxidation, J. Mater. Chem. A 6 (2018) 14717–14724, https://doi.org/10.1039/C8TA04471F.

[9] H. Yang, Z. Yu, S. Li, Q. Zhang, J. Jin, J. Ma, Ultrafine palladium-gold-phosphorus ternary alloyed nanoparticles anchored on ionic liquids-noncovalently functionalized carbon nanotubes with excellent electrocatalytic property for ethanol oxidation reaction in alkaline media, J. Catal. 353 (2017) 256–264, https://doi.org/10.1016/j.jcat.2017.07.025.

[10] L. Chen, L. Lu, H. Zhu, Y. Chen, Y. Huang, Y. Li, L. Wang, Improved ethanol electrooxidation performance by shortening Pd-Ni active site distance in Pd-Ni-P nanocatalysts, Nat. Commun. 8 (2017) 14136.

[11] E.A. Monyoncho, S. Ntais, N. Brazeau, J.J. Wu, C.L. Sun, E.A. Baranova, Role of the metal-oxide support in the catalytic activity of Pd nanoparticles for ethanol electrooxidation in alkaline media, ChemElectroChem 3 (2) (2016) 218–227, https://doi.org/10.1002/celc.201500432.

[12] G. Hu, F. Nitze, H.R. Barzegar, T. Sharifi, A. Mikołajczuk, C.W. Tai, A. Borodzinski, T. Wågberg, Palladium nanocrystals supported on helical carbon nanofibers for highly efficient electro-oxidation of formic acid, methanol and ethanol in alkaline electrolytes, J. Power Sources 209 (2012) 236–242, https://doi.org/10.1016/j.jpowsour.2012.02.080.

[13] A.L. Wang, X.J. He, X.F. Lu, H. Xu, Y.X. Tong, G.R. Li, Palladium-cobalt nanotube arrays supported on carbon fiber cloth as high-performance flexible electrocatalysts for ethanol oxidation, Angew. Chem. Int. Ed. Engl. 54 (12) (2015) 1–6, https://doi.org/10.1002/anie.201410792.

[14] L. Wang, Y. Wang, A. Li, Y. Yang, Q. Tang, H. Cao, T. Qi, C. Li, Electrocatalysis of carbon black- or poly(diallyldimethylammonium chloride)-functionalized activated carbon nanotubes-supported Pd-Tb towards methanol oxidation in alkaline media, J. Power Sources 257 (2014) 138–146, https://doi.org/10.1016/j.jpowsour.2014.01.109.

[15] L.X. Ding, A.L. Wang, G.R. Li, Z.Q. Liu, W.X. Zhao, C.Y. Su, Y.X. Tong, Porous Pt-Ni-P composite nanotube arrays: highly electroactive and durable catalysts for methanol electrooxidation, J. Am. Chem. Soc. 134 (13) (2012) 5730–5733, https://doi.org/10.1021/ja212206m.

[16] V. Celorrio, M.G. Montes de Oca, D. Plana, R. Moliner, D.J. Fermín, M.J. Lázaro, Electrochemical performance of Pd and Au-Pd core-shell nanoparticles on surface tailored carbon black as catalyst support, Int. J. Hydrogen Energ. 37 (8) (2012) 7152–7160, https://doi.org/10.1016/j.ijhydene.2011.12.014.

[17] A.K. Geim, K.S. Novoselov, The rise of graphene, Nanosci. Tech. (2009) 11–19, https://doi.org/10.1142/9789814287005_0002.

[18] L. Shao, T.W. Lin, G. Tobias, M.L.H. Green, A simple method for the containment and purification of filled open-ended single wall carbon nanotubes using C_{60} molecules, Chem. Commun. 18 (2008) 2164–2166.

[19] H. Zhang, Ultrathin two-dimensional nanomaterials, ACS Nano 9 (2015) 9439–9451, https://doi.org/10.1021/acsnano.5b05040.

[20] B. Zhang, X. Ni, W. Zhang, L. Shao, Q. Zhang, F. Girgsdies, C. Liang, R. Schlögl, D.S. Su, Structural rearrangements of Ru nanoparticles supported on carbon nanotubes under microwave irradiation, Chem. Commun. 47 (2011) 10716–10718.

[21] S. Bai, C. Wang, W. Jiang, N. Du, J. Li, J. Du, R. Long, Z. Li, Y. Xiong, Etching approach to hybrid structures of PtPd nanocages and graphene for efficient oxygen reduction reaction catalysts, Nano Res. 8 (9) (2015) 2789–2799.

[22] X. Huang, L. Shao, G.W. She, M. Wang, S. Chen, X.M. Meng, Catalyst-free synthesis of single crystalline ZnO nanonails with ultra-thin caps, CrystEngComm 14 (2012) 8330–8334.

[23] W. Zhang, W. Zheng, Single atom excels as the smallest functional material, Adv. Func. Mater. 26 (2016) 2988–2993, https://doi.org/10.1002/adfm.201600240.

[24] C. Zhang, W. Zhang, N.E. Drewett, X. Wang, S.J. Yoo, H. Wang, T. Deng, J. Kim, H. Chen, K. Huang, S. Feng, W. Zheng, Integrating catalysis of methane decomposition and electrocatalytic hydrogen evolution with Ni/Ce_O2 for improved hydrogen production efficiency, ChemSusChem 12 (2019) 1000–1010, https://doi.org/10.1002/cssc.201802618.

[25] M.M. Demir, M.A. Gulgun, Y.Z. Menceloglu, B. Erman, S.S. Abramchuk, E.E. Makhaeva, A.R. Khokhlov, V.G. Matveeva, M.G. Sulman, Palladium nanoparticles by electrospinning from Poly(acrylonitrile-co-acrylic acid)-$PdCl_2$ solutions. Relations between preparation conditions, particle Size, and catalytic activity, Macromolecules 37 (2004) 1787–1792, https://doi.org/10.1021/ma035163x.

[26] P. Wang, G. Zhang, H. Jiao, L. Liu, X. Deng, Y. Chen, X. Zheng, Pd/graphene nanocomposite as highly active catalyst for the Heck reactions, Appl. Catal. A 489 (2015) 188–192, https://doi.org/10.1016/j.apcata.2014.10.044.

[27] H. Gao, L. He, Y. Zhang, S. Zhang, L. Wang, Facile synthesis of Pt nanoparticles supported on graphene/Vulcan XC-72 carbon and their application for methanol oxidation, Ionics 23 (2) (2016) 435–442.

[28] M.M. Lucchese, F. Stavale, E.H.M. Ferreira, C. Vilani, M.V.O. Moutinho, R.B. Capaz, C.A. Achete, A. Jorio, Quantifying ion-induced defects and Raman relaxation length in graphene, Carbon 48 (5) (2010) 1592–1597, https://doi.org/10.1016/j.carbon.2009.12.057.

[29] W. Zhou, J. Lee, Particle size effects in Pd-catalyzed electrooxidation of formic acid, J. Phys. Chem. C 112 (2008) 3789–3793, https://doi.org/10.1021/jp077068m.

[30] H. Meng, S. Sun, J.P. Masse, J.P. Dodelet, Electrosynthesis of Pd single-crystal

nanothorns and their application in the oxidation of formic acid, Chem. Mater. 20 (2008) 6998–7002, https://doi.org/10.1021/cm8014513.
[31] H.F. Wang, W.E. Kaden, R. Dowler, M. Sterrer, H.J. Freund, Model oxide-supported metal catalysts-comparison of ultrahigh vacuum and solution based preparation of Pd nanoparticles on a single-crystalline oxide substrate, Phys. Chem. Chem. Phys. 14 (32) (2012) 11525–11533.
[32] W.H. Lee, P.J. Reucroft, Vapor adsorption on coal- and wood-based chemically activated carbons: (I) Surface oxidation states and adsorption of H_2O, Carbon 37 (1) (2007) 7–14, https://doi.org/10.1016/S0008-6223(98)00181-X.
[33] K.A. Wepasnick, B.A. Smith, J.L. Bitter, D. Howard Fairbrother, Chemical and structural characterization of carbon nanotube surfaces, Anal. Bioanal. Chem. 396 (3) (2010) 1003–1014.
[34] K. Zhang, B.T. Ang, L.L. Zhang, X.S. Zhao, J. Wu, Pyrolyzed graphene oxide/resorcinol-formaldehyde resin composites as high-performance supercapacitor electrodes, J. Mater. Chem. 21 (8) (2011) 2663–2670.
[35] Z.X. Liang, T.S. Zhao, J.B. Xu, L.D. Zhu, Mechanism study of the ethanol oxidation reaction on palladium in alkaline media, Electrochimica Acta 54 (2009) 2203–2208, https://doi.org/10.1016/j.electacta.2008.10.034.
[36] R. Pattabiraman, Electrochemical investigations on carbon supported palladium catalysts, Appl. Catal. A 153 (1997) 9–20, https://doi.org/10.1016/S0926-860X(96)00327-4.
[37] X. Chen, B. Su, G. Wu, C.J. Yang, Z. Zhuang, X. Wang, X. Chen, Platinum nanoflowers supported on graphene oxide nanosheets: their green synthesis, growth mechanism, and advanced electrocatalytic properties for methanol oxidation, J. Mater. Chem. 22 (2012) 11284–11289.
[38] H. Hu, Z. Zhao, W. Wan, Y. Gogotsi, J. Qiu, Ultralight and highly compressible graphene aerogels, Adv. Mater. 25 (15) (2013) 2219–2223, https://doi.org/10.1002/adma.201204530.
[39] J. Mao, J. Iocozzia, J. Huang, K. Meng, Y. Lai, Z. Lin, Graphene aerogels for efficient energy storage and conversion, Energ. Environ. Sci. 11 (4) (2018) 772–799.
[40] C. Batchelor-McAuley, L. Shao, G.G. Wildgoose, M.L.H. Green, R.G. Compton, An electrochemical comparison of manganese dioxide microparticles versus α and β manganese dioxide nanorods: mechanistic and electrocatalytic behaviour, New J. Chem. 32 (2008) 1195–1203.
[41] G.R. Zhang, B.Q. Xu, Surprisingly strong effect of stabilizer on the properties of Au nanoparticles and Pt^Au nanostructures in electrocatalysis, Nanoscale 2 (12) (2010) 2798–2804.
[42] S. Kabir, A. Serov, K. Artyushkova, P. Atanassov, Design of novel graphene materials as a support for palladium nanoparticles: highly active catalysts towards ethanol electrooxidation, Electrochim. Acta 203 (2016) 144–153, https://doi.org/10.1016/j.electacta.2016.04.026.
[43] J.C. Ng, C.Y. Tan, B.H. Ong, A. Matsuda, Effect of synthesis methods on methanol oxidation reaction on reduced graphene oxide supported palladium electrocatalysts, Procedia Eng. 184 (2017) 587–594, https://doi.org/10.1016/j.proeng.2017.04.143.
[44] Z. Zhuang, W. Chen, Ultra-low loading of Pd_5 nanoclusters on carbon nanotubes as bifunctional electrocatalysts for the oxygen reduction reaction and the ethanol oxidation reaction, J. Colloid Interface Sci. 538 (2019) 699–708, https://doi.org/10.1016/j.jcis.2018.12.015.